The Meteoritical Society

Meteoritics & Planetary Science 44, Nr 11, 1787–1796 (2009)
Abstract available online at http://meteoritics.org

Interpreting the I-Xe system in individual silicate grains from Toluca IAB

O. V. PRAVDIVTSEVA[1*], A. P. MESHIK[1], C. M. HOHENBERG[1], and M. PETAEV[2]

[1]Washington University, Box 1105, One Brookings Drive, Saint Louis, Missouri 63117, USA
[2]Department of Earth and Planetary Sciences, Harvard University, 20 Oxford St., Hoffman 208 Cambridge, Massachusetts 02138, USA
[*]Corresponding author. E-mail: olga@physics.wustl.edu

(Received 24 March 2009; revision accepted 25 August 2009)

Abstract–Detailed isotopic and mineralogical studies of silicate inclusions separated from a troilite nodule of the Toluca IAB iron meteorite reveal the presence of radiogenic ^{129}Xe in chlorapatite, plagioclase, perryite, and pyroxene grains. Subsequent I-Xe studies of 32 neutron-irradiated pyroxene grains indicate that high-Mg and low-Mg pyroxenes have distinctive I-Xe signatures. The I-Xe system in high-Mg pyroxenes closed at 4560.5 ± 2.4 Ma, probably reflecting exsolution of silicates from the melt, while the low-Mg pyroxenes closed at 4552.0 ± 3.7 Ma, 8.5 Ma later, providing a means for determining the cooling rate at the time of exsolution. If the host Toluca graphite-troilite-rich inclusion formed after the breakup and reassembly of the IAB parent body as has been suggested, the I-Xe ages of the high-Mg pyroxenes separated from this inclusions indicate that this catastrophic impact occurred not later than 4560.5 Ma, 6.7 Ma after formation of CAIs. The cooling rate at the time of silicates exsolution in Toluca is 14.5 ± 10.0 °C/Ma.

INTRODUCTION

IAB iron meteorites have complicated textures and chemical-mineralogical features that indicate a complex history for the IAB parent body. They commonly contain abundant silicate inclusions with chondritic mineralogy embedded in the metal phase. In an attempt to create the least complicated formation scenario, Benedix et al. (2000) explored a hypothesis in which the parent body began to differentiate, but the differentiation process was interrupted by a catastrophic impact with gravitational reassembly responsible for the mixing of different lithologies from different regions in the parent body. Although this hypothesis does not completely explain all properties of these rocks, it does explain the mixing of solid silicates with molten metal and slow (<700 °C/Ma) cooling rates for the buried, reassembled debris.

Wasson and Kallemeyn (2002) argued that abundance of fine (≤100 μm) silicates in low-Au irons points towards fast cooling, so the viscosity of the melt became large on a time scale short compared to the time necessary for silicate grains to separate from the melt. Fast cooling could be also responsible for the small sizes of the γ–iron crystals parental to the Widmanstätten pattern and for the limited thermal effects recorded in the silicates, including abundant primordial rare gases (Schultz and Franke 2000). Similar element-Au trends suggested for the different groups of IAB irons, and for related meteorites, could also be the results of similar processes instigated by independent impact events that occurred either at separate locations on the same asteroid or on separate but compositionally similar asteroids (Wasson and Kallemeyn 2002).

IABs cooling rates (~25–70 °C/Ma), obtained from the Widmanstätten structures in the metal phases and inferred for metal grains in chondritic inclusions, were consistent for the same meteorites (Herpfer et al. 1994), and correlated well with their Ni content. Based on these relatively slow cooling rates, the spread in apparent radiometric ages that is observed and the proposed complex formation scenarios (Benedix et al. 2000; Wasson and Kallemeyn 2002; Bogard et al. 2005) suggested that different chronometers might record different events in the history of the IAB parent body, and that the I-Xe system was not reset during metamorphism reflected in much younger Ar-Ar and Sm-Nd ages. In this work we present new I-Xe data for the Toluca IAB iron meteorite. Toluca is an optimum object for this study. It is not heavily shocked with the troilite nodules rarely showing any evidence for micro-melting (Buchwald 1975), and the presence of radiogenic noble gases indicates that the early records have been preserved in at least some phases (Bogard et al. 1968).

^{129}I decays to radiogenic ^{129}Xe (denoted ^{129*}Xe), forming the basis for I-Xe dating (Hohenberg and Pravdivtseva 2008). The chronometric parameter here is the ratio of stable ^{127}I to ^{129}I at the time of Xe closure. A tracer for ^{127}I is iodine-derived ^{128}Xe (denoted ^{128*}Xe), produced by neutron capture on ^{127}I in a reactor, so the ^{129*}Xe/^{128*}Xe ratio, properly

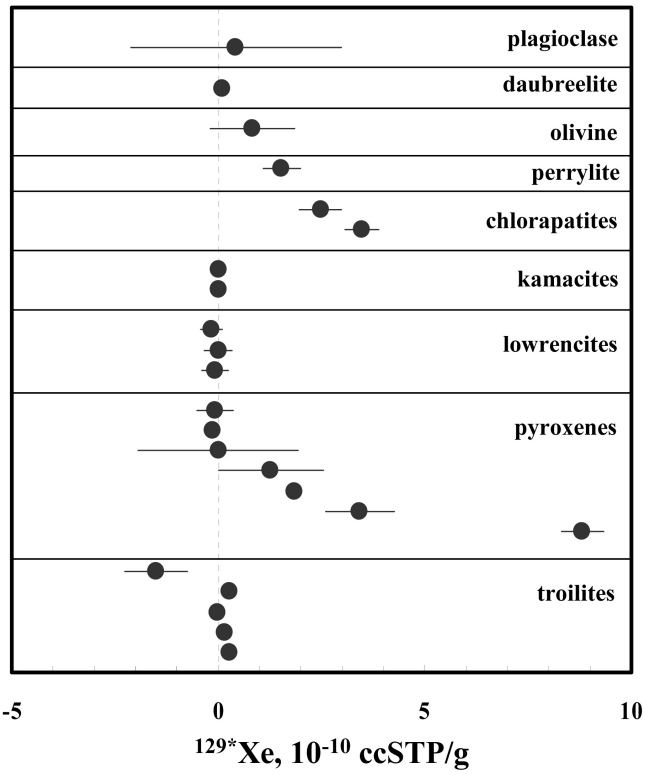

Fig. 1. Concentrations of radiogenic ^{129}Xe in unirradiated individual mineral grains separated from a Toluca (IAB) troilite nodule.

monitored, provides the chronometry. Direct monitoring of the neutron capture probability is impractical for several reasons. A calibration procedure by means of a reference meteorite standard yields the highest precision of both relative (in our case to the irradiation standard Shallowater) and absolute closure times. In I-Xe dating Xe isotopes released in step-wise heating result in linear isochrons, mixtures of "trapped" Xe and unique values of ^{129*}Xe/^{128*}Xe, defining the values for the ^{129}I/^{127}I at closure (Hohenberg and Pravdivtseva 2008).

SAMPLE PREPARATION

Toluca fragment USNM 931, described in detail by Benedix et al. (2000), was obtained from the Smithsonian National History Museum. This fragment contained remnants of three troilite inclusions, one with abundant silicate grains of different morphology. From this troilite nodule we handpicked 23 grains which were placed on an SEM stub with carbon tape for SEM studies with energy-dispersive X-ray analyses on a JEOL-840A scanning electron microscope providing phase identification (Fig. 1) and quantification of phase purity. The grains were then removed from the SEM mount, washed in methanol and de-ionized water, and then desiccated overnight. Each grain was weighed twice using a Cahn C-31 microbalance with an additional 24 hours of drying between weighings to confirm dehydration by weight reproducibility. They were then loaded onto the target mount for laser extraction and subsequent xenon isotopic analysis. The target mount for laser extraction from the individual grains consists of a matrix of 1 mm holes (one grain per hole) in an Al laser stub. This stub fits inside of the laser extraction cell with a Pyrex view-port for laser entry and optical viewing. This cell is attached by flexible stainless steel tubing to the gas preparation system of an ion-counting noble gas mass spectrometer (Hohenberg 1980).

Typically, total degassing by complete melting (confirmed by spherical droplet formation) of an average-sized (~20 μg) grain takes about five seconds with a 100 W CW Nd-YAG laser (1.06 μm) focused on the grain. The actual laser power delivered to the grain (<25 W) is controlled by a pair of water-cooled Glan-Thompson air-spaced polarizers with continuously variable orientations and adjusted in real time for rapid melting. "Hot blanks", typically ~2×10^{-15} cm^3 STP ^{132}Xe, are measured at similar laser power levels directed into empty holes in the stub so any parasitic heating effects are replicated.

Trapped Xe refers to the component originally incorporated in the mineral, with an isotopic composition typically referred to as "planetary" Xe. We use OC Xe (Lavielle and Marti 1992) for the trapped composition, but for most I-Xe applications trapped Xe is sufficiently close to other prevalent Xe components, even atmospheric Xe, that this choice in not important. For typical I-Xe dating, trapped Xe is never a consideration since trapped Xe always forms one endpoint of the I-Xe isochron. However, for this study we want to determine the iodine carrier phase, so the ^{129*}Xe content of each grain was found by removing the trapped Xe component (Fig. 1). None of the troilite, kamacite, olivine or daubreelite grains contained detectable ^{129*}Xe. The single plagioclase grain contained a significant fraction of trapped Xe and thus a correspondingly larger uncertainty of the ^{129*}Xe content. Both chlorapatites, at least two pyroxenes, and one perryite grain were dominated by ^{129*}Xe. The apparent slight negative quantity of radiogenic ^{129}Xe in one of the troilites is an artifact due to the large correction for trapped Xe. Three lawrencite grains, a terrestrial weathering product, separated from the same Toluca troilite nodule, were analyzed as a reference and contained no ^{129*}Xe.

Although at least three different silicates contained clear amounts of ^{129*}Xe, and were thus potentially suitable for the I-Xe studies, we focused on the pyroxene grains since they were generally larger in size and more abundant. Moreover, the clear correlation between the Mg/(Fe+Mg) ratios and the concentration of ^{129*}Xe that was observed in these unirradiated pyroxenes (Pravdivtseva et al. 1998) suggested that thermochronological studies of these silicates may be productive (McDougall and Harrison 1999).

We separated 63 pyroxene grains from the same troilite nodule of the Toluca fragment USNM 931. After the identification procedure described above, the concentrations of Fe, Mg, Si, and Al were determined from their X-ray

Table 1. Individual Toluca pyroxene grains sorted according their Mg-numbers.

									Free fit slopes		Forced through OC slopes	
	Grain #	Mg/(Mg+Fe) Mole corr.	FeS	Plag	Cpx	Opx	Ol	Qtz	"Best fit" points		"Best fit" points	
1	*14*	*1.0000*	*31.48*	*0.00*	*0.44*	*58.76*	*0.00*	*9.32*				
2	*21*	*1.0000*	*22.97*	*0.00*	*0.49*	*70.45*	*0.00*	*6.09*				
3	*45*	*1.0000*	*22.72*	*0.00*	*0.67*	*69.00*	*0.00*	*7.61*				
4	*61*	*1.0000*	*19.21*	*6.18*	*0.00*	*53.98*	*0.00*	*20.64*				
5	*55*	*0.9776*	*18.94*	*0.00*	*0.58*	*64.54*	*0.00*	*15.94*				
6	20*	0.9736	0.94	0.00	6.13	80.34	0.00	12.59				
7	*10*	*0.9565*	*11.89*	*0.00*	*0.95*	*72.31*	*0.00*	*14.85*				
8	36*	0.9536	3.21	0.00	0.85	87.75	0.00	8.19				
9	63*	0.9496	4.11	0.00	0.52	84.65	10.72	0.00				
10	28*	0.9464	3.87	0.00	1.09	87.62	0.00	7.42				
11	46*	0.9315	8.42	7.88	0.00	72.12	0.00	11.59				
12	17*	0.9279	3.03	0.00	1.00	88.45	0.00	7.52	0.741 ± 0.092		0.6364 ± 0.050	
13	*12*	*0.9242*	*10.15*	*1.35*	*0.69*	*78.26*	*9.55*	*0.00*				
14	47*	0.9231	3.88	0.00	1.12	73.56	0.00	21.45	0.770 ± 0.093		0.697 ± 0.045	
15	15*	0.9123	2.92	0.00	0.93	93.70	0.00	2.45	0.793 ± 0.087		0.689 ± 0.045	
16	5*	0.9041	5.12	0.00	0.56	93.18	1.15	0.00	0.754 ± 0.062		0.693 ± 0.037	
17	29*	0.8925	4.55	4.54	0.20	82.05	0.00	8.66	0.7674 ± 0.059	0.75 ± 0.11	0.705 ± 0.034	0.837 ± 0.055
18	11	0.8922	5.62	0.00	1.00	90.54	0.00	2.83				
19	39	0.8919	1.29	0.00	0.68	94.39	0.00	3.64				
20	33	0.8719	5.71	0.00	0.60	92.82	0.00	0.86				
21	32	0.8715	6.15	0.00	1.01	84.40	0.00	8.45				
22	19	0.8566	5.61	0.00	1.13	92.93	0.00	0.32				
23	1	0.8461	4.78	0.00	1.15	90.11	0.00	3.96				
24	31	0.8427	2.43	0.00	1.11	90.01	6.45	0.00				
25	35†	0.8304	4.02	0.00	1.24	93.27	1.47	0.00	0.519 ± 0.092		0.524± 0.041	
26	38†	0.8098	4.68	0.00	1.18	88.47	5.68	0.00				
27	24†	0.7958	6.10	0.00	1.08	83.80	9.01	0.00				
28	54†	0.7904	3.52	0.00	1.67	89.02	5.80	0.00				
29	*41*	*0.7877*	*10.55*	*19.40*	*0.00*	*59.94*	*0.00*	*10.12*				
30	56†	0.7695	8.38	15.68	0.00	61.85	0.00	14.09				
31	*44*	*0.7670*	*39.87*	*0.00*	*0.56*	*46.43*	*0.00*	*13.14*				
32	27†	0.6994	8.32	0.00	1.57	86.72	0.00	3.39				

The slope of the Shallowater isochron is 0.8468 ± 0.0052. *High Mg-number grains. †Low Mg-number grains.

spectra, which also revealed the presence of Ni and Cr in some grains in smaller amounts (<1% atomic). Sulfur concentrations were measured to monitor possible troilite intergrowth (its corresponding Fe would corrupt the Mg/(Fe+Mg) trends). Although the high Mg/(Fe+Mg) pyroxene grains were the more abundant, we selected 32 grains of a more uniform range, exhibiting a continuous trend of Mg/(Fe+Mg) ratios so we could clearly delineate the correlation of this trend with their ^{129*}Xe contents (Table 1).

The selected grains, along with Shallowater enstatite (reference standard), were weighed and sealed under vacuum in fused-quartz ampoules for neutron irradiation, receiving ≈2 × 10^{19} n/cm^2 as part of the SLC-14 capsule at the University of Missouri Research Reactor (UMRR). To control the uniformity of neutron fluence the samples were placed in a fixed plane at the center of the vertical neutron profile in the pool of the reactor to minimize any vertical gradient, and the capsule was continuously rotated to eliminate any x-y gradient. To monitor any possible fluence variations, neutron doses were monitored by Co-doped Ni flux wires placed strategically around the perimeter of the irradiation capsule interspersed with the sample vials. Subsequent counting of these flux wires confirmed neutron variations of <1% among the samples. After irradiation the grains were loaded into individual holes in target mount for laser extraction and mass spectrometry. The samples studied here were too small to allow conventional I-Xe step-wise extractions, so Xe was extracted individually from each grain by total melting, as described for the unirradiated grains, and the xenon isotopic compositions were measured by ion counting mass-spectrometry (Hohenberg 1980).

RESULTS

Xenon isotopic compositions for individual Toluca pyroxene grains are shown in Table 2. ^{132}Xe concentrations

Table 2. Xenon isotopic compositions for individual Toluca pyroxene grains.

Grain, #	Weight, μgm	$^{132}Xe \times 10^{-10}$, cm^3 STP/g	$^{132}Xe \equiv 100$							
			^{124}Xe	^{126}Xe	^{128}Xe	^{129}Xe	^{130}Xe	^{131}Xe	^{134}Xe	^{136}Xe
1	12.3	336.7	0.9781	0.7381	224.316	235.69	18.415	254.112	37.012	43.737
			0.7813	0.5745	20.202	16.25	2.738	21.508	7.044	3.546
5	23.1	63.3	2.9797	–0.4473	397.073	349.80	23.870	181.282	78.033	37.558
			1.5035	1.4040	19.480	20.13	3.893	11.514	7.135	7.012
10	46.0	230.2	0.8316	0.8252	133.565	338.87	16.010	104.561	44.403	31.340
			0.3637	0.4688	8.700	16.72	1.923	8.543	3.030	2.233
11	21.6	35.6	4.9606	4.6490	191.466	120.63	4.408	104.221	44.518	35.147
			3.2966	1.7844	22.544	15.28	4.985	23.939	12.699	9.423
12	23.6	341.2	0.9123	0.5354	251.900	312.01	11.952	117.033	32.634	29.894
			0.5366	0.5114	9.645	17.32	2.802	7.412	2.766	3.314
14	28.8	204.6	0.7649	1.4451	218.427	223.30	14.473	195.014	34.652	23.960
			0.6487	0.8830	10.984	12.10	1.601	12.988	3.655	3.033
15	16.5	73.2	1.1773	1.0396	71.317	118.781	10.845	2206.287	49.694	35.122
			2.5612	1.6214	10.215	15.46	4.119	230.452	11.068	8.082
17	18.2	85.8	–1.8594	–0.0306	457.032	467.57	23.378	327.042	47.560	43.908
			1.6591	1.1594	26.869	43.88	3.859	32.824	7.227	6.692
19	12.3	162.0	–0.1162	0.4125	148.960	194.10	12.856	126.895	33.884	42.036
			1.1303	1.3479	10.187	15.63	4.143	16.680	9.516	8.264
20	7.0	237.4	–0.8960	–0.5926	239.594	287.50	12.580	106.076	47.201	29.464
			1.2048	1.4037	21.727	38.90	2.923	18.903	7.041	6.260
21	18.2	154.3	–1.3925	–3.0148	353.606	342.61	18.163	244.281	37.216	33.309
			1.0405	0.7206	27.710	22.27	2.465	24.537	6.488	7.127
24	12.1	152.0	2.4142	2.8550	212.121	229.43	20.984	168.695	41.546	20.180
			2.3348	2.0022	13.905	23.73	4.860	17.312	8.619	6.188
27	7.1	345.5	1.7268	0.3660	225.746	209.64	14.187	311.729	41.585	26.586
			1.0332	0.7963	19.984	12.22	2.896	25.404	5.223	4.495
28	11.0	126.5	–2.7845	–0.7689	97.602	187.18	20.673	360.098	37.023	46.914
			1.8563	2.3837	13.191	21.29	2.507	44.501	4.494	7.700
29	14.4	179.9	0.1343	0.6636	339.750	353.074	23.709	176.026	47.735	49.417
			1.0425	0.9605	22.030	25.82	3.877	17.152	5.541	5.956
31	19.4	87.9	0.8115	1.4733	294.563	270.91	15.983	248.049	43.147	32.302
			1.6993	1.2197	21.695	23.29	3.947	24.495	7.698	7.873
32	12.4	137.5	1.0618	0.6455	171.976	177.82	19.132	180.334	51.169	46.685
			1.4544	1.2056	16.782	19.86	4.662	19.659	6.503	10.623
33	12.3	148.7	0.8061	3.5166	263.378	219.89	15.968	182.866	37.822	15.753
			1.1948	1.5702	27.196	23.96	2.179	22.280	6.000	3.795
35	6.0	357.8	–1.4088	0.7902	54.596	97.44	14.553	89.217	49.721	40.649
			0.8293	1.0441	6.155	8.13	2.649	11.422	6.165	6.977
36	12.4	76.5	5.2407	–3.8534	69.731	125.12	19.940	678.432	34.903	39.577
			2.0866	1.6905	7.052	13.97	5.246	83.612	8.929	7.957
38	13.7	118.0	0.3052	0.3437	171.528	178.25	11.358	249.692	44.083	30.591
			0.8984	0.7571	9.111	13.51	2.545	21.180	7.271	5.881
39	18.3	200.6	0.8628	–0.3174	223.383	230.73	16.909	152.556	51.185	39.912
			0.8191	0.6141	11.702	12.44	2.123	14.597	5.647	5.130
41	19.9	93.1	0.0545	–0.3704	245.637	290.35	21.182	110.574	31.881	34.377
			0.8697	1.7315	20.459	22.83	4.009	14.798	6.489	6.688
44	43.9	131.0	–0.8264	0.3923	365.629	310.15	17.452	674.700	32.755	30.838
			0.4538	0.5250	14.768	15.14	2.271	26.632	2.567	3.630
45	110.2	39.7	2.9114	0.4557	220.659	231.91	21.119	167.364	55.487	45.752
			0.8484	0.3621	13.408	17.24	2.305	11.604	4.723	4.031
46	41.8	256.5	0.3241	1.6079	276.010	271.25	23.821	381.574	22.181	35.541
			1.0385	1.6124	20.736	26.54	9.262	75.396	8.731	15.014
47	16.8	258.6	0.5266	0.3845	162.675	241.53	17.015	552.815	43.825	36.315
			0.2134	0.6341	9.171	13.76	2.130	34.534	4.766	4.158
54	18.5	243.7	0.2405	2.3844	66.976	129.04	16.753	117.133	48.847	32.590
			0.3166	0.3530	5.767	9.28	2.396	5.176	5.052	3.657
55	45.0	345.8	0.1134	0.5769	160.669	149.81	17.295	254.773	35.577	27.797
			0.2514	0.2954	4.436	4.62	1.216	9.901	2.194	2.485
56	9.2	276.8	1.0545	–1.0027	252.660	231.14	21.841	376.714	42.944	37.165
			0.9571	0.7220	17.792	13.67	2.723	28.935	4.850	4.152
61	19.8	200.0	1.5907	–0.0552	298.111	246.87	20.143	368.844	37.684	32.587
			1.1475	0.8046	18.208	18.01	2.356	30.503	7.599	5.070
63	25.5	203.1	0.1339	0.3575	241.633	225.21	22.000	608.947	39.690	40.013
			0.6749	0.5048	14.325	15.48	1.883	39.879	3.840	5.125

range from 35.6×10^{-12} to 357.8×10^{-12} ccSTP/g of ^{132}Xe, with average value 184.5×10^{-12} ccSTP/g, in agreement with the previously reported data for Mundrabilla (IAB) silicates and etched Pitts (IAB) silicates (Niemeyer 1979a). ^{129*}Xe was variable (loosely correlated with the Mg/(Fe+Mg) ratio with the amounts consistent with those observed by Niemeyer [1979a]).

In I-Xe studies using step-wise heating, the data are typically presented in three-isotope correlation plots where the ^{129}Xe/^{132}Xe ratios released in the incremental fractions are plotted versus the ^{128}Xe/^{132}Xe ratios. The choice of normalization isotope (^{132}Xe or ^{130}Xe) depends upon the precision of these ratios, as corrected for (usually small) fission or spallation contributions. The low-temperature extractions (from the less retentive sites) usually contain uncorrelated xenon due to the partial loss of the radiogenic ^{129}Xe or superficial iodine contamination. These low temperature points in step-wise extraction are not included in the isochron, the slope of which provides the I-Xe age normalized by the Shallowater reference standard.

For these Toluca pyroxene grains the Xe is released with laser volatilization in one step and thus it contains both correlated and uncorrelated iodine-derived Xe. The extraction cell was heated to 220 °C prior to the analysis to remove superficial atmospheric contributions. But since pyroxene usually yields a linear isochron in the temperature range of 1200 to 1800 °C, the pre-heating temperature is insufficient for completely separating uncorrelated and correlated iodine-derived Xe. Each experimental point on three isotope plot (Fig. 2a) therefore represents all of the xenon released from each of the Toluca grains, not just the correlated portion. However, as will be discussed later, this is a small effect and does not affect the results.

Small corrections were made for the minor amounts of ^{132}Xe produced by neutron fission of ^{235}U in the reactor. The maximum fission contribution (grain #29) was 27%, while for all other samples it was much less, varying from 0.2% to 10%. Fission corrections were made by partitioning the measured ^{134}Xe/^{132}Xe ratios between that of ^{235}U fission and that in nominal trapped Xe. Although both ^{130}Xe and ^{132}Xe normalizations give the same ages, normalization to (fission-corrected) ^{132}Xe is usually preferred because of the smaller uncertainties it yields.

The experimental data from all irradiated Toluca grains are shown on Fig. 2a. If the iodine-xenon systems in a range of grains closed at the same time, and there were no uncorrelated Xe, the xenon released from these grains would form an isochron on the three isotope plot, a mixing line between trapped Xe and iodine-derived Xe. Any uncorrelated xenon, with its excess ^{128*}Xe, would move the experimental points to the right in the figure. However, in previous studies of samples whose radiogenic fractions are as large as these, the I-Xe record is usually preserved and most of the iodine-derived Xe is correlated with an average of about 80% forming the isochron (Hohenberg et al. 2004). Although small contributions from uncorrelated iodine can vary from grain-to-grain, the resulting points will scatter somewhat, but after eliminating obvious outliers, the slope of the isochron will not be affected very much and provide a reliable I-Xe age, although with somewhat less precision. That these groups of grains form fairly good isochrons (linear arrays in Figs. 2b, and 2c) argues to this point.

To investigate the correlation between closure times of the I-Xe system in the pyroxene grains with varying Mg, suggested by the observations of unirradiated pyroxenes (Pravdivtseva et al. 1998), we sorted the grains according to their Mg/(Mg+Fe) ratios (Table 1). Since the unirradiated troilite grains in our preliminary study demonstrated presence of variable amounts of ^{129*}Xe in troilite, we excluded 9 grains with troilite contents higher than 10% (shown in italics) from the calculations of the apparent isochron slopes. Slopes of the isochrons for the high-Mg grains (column 12, Table 1) were calculated as following: The first number in column 10 is the slope of the line formed by the first six grains with the highest Mg-number (#20, #36, #63, #28, #46 and #17). Then we add more data, grain-by-grain, so the next slope (the next number in column 10) is calculated for the line formed by the first 7 grains and so on, down to grain #29, the 10th grain. At this point the uncertainty of the slope reaches its minimum. We thus consider here the 10 grains with the highest Mg/(Mg+Fe) ratios to be Mg-rich. Among this group of pyroxenes the Mg/(Mg+Fe) ratio varies by about 8%. Grain #27 has the lowest Mg-number of 0.6994 and that is about 10% lower than that of the next lowest grain, #56. Because of that difference, we adopted an 8% range for the increase in Mg/(Mg+Fe) ratios starting with grain #56. This gives us 6 grains (including grain #27) for the apparent low-Mg isochron. The smaller number of grains for the low-Mg pyroxenes isochron reflects the low abundance of these grains in this Toluca nodule. The grains with higher Fe content were generally smaller, more brittle and thus more difficult to separate.

All of the values in column 10 are calculated for the correlation lines forced through the OC point, thus reducing false trends due to a few outliers. As we mentioned, the presence of uncorrelated Xe would move the experimental points to the right, away from the isochron in Fig. 2. To investigate this effect we also calculated slopes for free-fit correlation lines (not forced through OC), displayed in Fig. 2 and in column 10 (Table 1).

Slope values change gradually when increasing numbers of grains are used to define the correlation line. For the high-Mg pyroxenes when 6 grains define the line, the maximum spread of ^{128}Xe/^{132}Xe and ^{129}Xe/^{132}Xe ratios is achieved. The addition of 4 more points, improves the uncertainty of the apparent isochron slope, giving us 0.705 ± 0.034, but does not significantly affect the slope value itself. Similar behavior can be observed when the correlation lines are not forced through OC, resulting in a slope of 0.767 ± 0.059. We then calculated

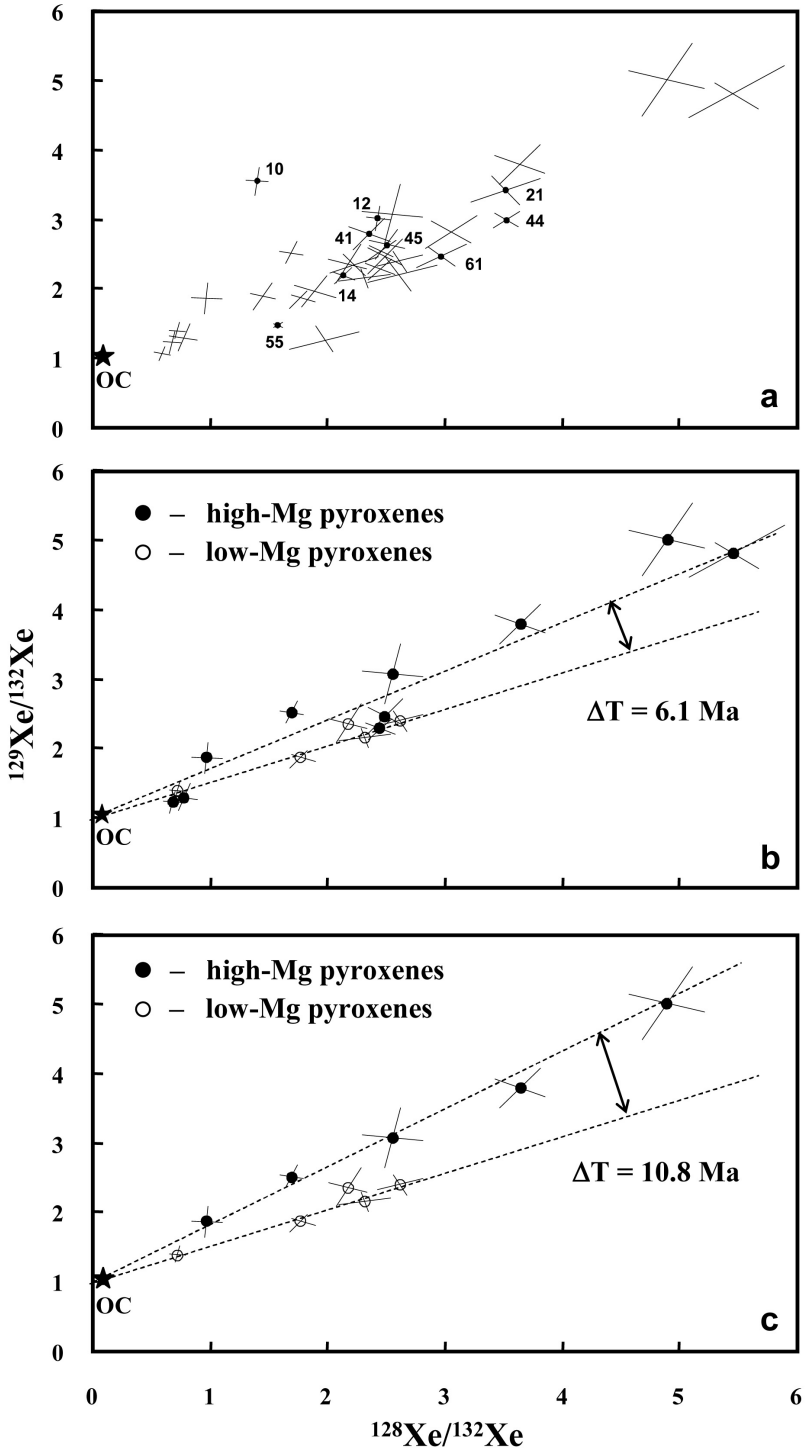

Fig. 2. Three isotope plots for individual pyroxene grains, separated from a Toluca IAB graphite-rich troilite nodule. Because of the presence of fission-produced Xe, the best isotope of normalization would have been ^{130}Xe. However, since these were small grains, the lower abundance of ^{130}Xe compromises the precision, so we normalize to ^{132}Xe after correction for fission contributions, based upon the observed ^{134}Xe/^{132}Xe ratios. This introduces correlated errors which show up here as oblique 1σ error bars. a) Data points for all of the analyzed grains shown. Numbered grains have troilite content higher than 10% and were excluded from isochron slope determinations. Different I-Xe ages are indicated for these grains depending upon their Mg/(Mg+Fe) ratios. b) These apparent isochrons show the smallest possible age difference between the two groups of Toluca grains (see text): with higher (solid circles) and with lower (open circles) Mg/(Mg+Fe) ratios. c) The isochrons shown here are derived from the "best fit" lines of these two groups of Toluca grains: with higher (solid circles) and lower (open circles) Mg/(Mg+Fe) numbers.

the free fit and the fit forced through OC for the 5 "best fit" grains from the high-Mg group, resulting in slopes of 0.75 ± 0.11 and 0.837 ± 0.055, respectively (Fig. 2c), which excluded some grains anomalously to the right of the isochron, suggesting the presence of significant uncorrelated Xe. Among these were grains #36, #15 and #46. Grains #36 and #15 had compositions close to trapped, thus very low in ^{129}*Xe, and grain #46 had ~8% plagioclase.

We now have 4 values for the slopes of I-Xe correlation lines for the high-Mg pyroxenes. Those forced through OC component point yielded the highest values, with "best fit" points providing steepest apparent isochron (slope 0.837 ± 0.055) and the value based on all 10 grains being the lowest 0.705 ± 0.034. Slopes of the free fit correlation lines vary less, from 0.75 ± 0.11 for "best fit" 5 points slope and 0.767 ± 0.059 for 10 points. This suggests that the free fit may best represent that I-Xe age since the small addition of uncorrelated Xe is averaged out (the line moves collectively to the right, rather than being forced to pivot about OC, thus increasing its slope).

Values for the slopes of the correlation lines formed by the low-Mg pyroxenes were obtained in a straight-forward manner. Since grain #35 demonstrated extremely low ^{129*}Xe content, comparable with planetary xenon, we did not use this grain in the calculations. It left us with only 5 grains in this set of samples. As with the high-Mg grains, we calculated the slopes for two apparent isochrons, forced through OC component point and free fit lines. These provided more consistent I-Xe ages, with slopes that differ by only 1% (Table 1).

Relative Ages of Mineral Groups and Absolute I-Xe Ages of Toluca Silicates

The free fit correlation line using "best fit" grains probably provides the most accurate value for the slope of the high-Mg pyroxenes isochron, and hence the closure time of the I-Xe system in high-Mg pyroxenes. Using different fits, and different grain selections among the group, a range of closure times 0.3–4.2 Ma after Shallowater were found (the extreme values here were correlation lines forced through the OC composition), but the most probable was the free-fit isochron yielding closure 2.8 ± 2.4 Ma after Shallowater. For the low-Mg group, the I-Xe closure time is well-determined at 11.3 ± 3.7 Ma after Shallowater. The closure time difference between the high- and low-Mg groups is then set at 8.5 ± 4.4 Ma (using free fit correlation lines).

With absolute age of Shallowater enstatite determined to be 4563.3 ± 0.4 Ma (Gilmour et al. 2004, 2006), this sets closure of the I-Xe system in high-Mg pyroxenes at 4560.5 ± 2.4 Ma, and the low-Mg pyroxenes at 4552.0 ± 3.7, well within the previously reported range of I-Xe ages for IAB iron meteorites (Niemeyer 1979a; Bogard et al. 2005).

Interpretation

The IAB iron meteorites are famous for their puzzling combination of metal matrix and often abundant silicate-bearing inclusions. A number of hypotheses have been postulated for the formation of the IAB iron meteorites. According to the latest scenario by Benedix et al. (2000), IAB iron and winonaite meteorites were part of the same chondritic parent body, one that was heated by a non-collisional heat source leading to partial melting and incomplete differentiation. A subsequent catastrophic impact caused fragmentation and then reassembly of the partially melted parent body, resulting in extensive mixing of solid silicates, molten metal, and sulfides. If such impacts were common events in the early solar system (Scott 2004), IAB meteorites could possibly experience more than one impact event. This makes comparisons of the chronological data from different meteorites quite difficult, and even more difficult comparison of ages provided by different chronometers for samples from different IAB meteorites.

Ar-Ar ages of 10 IAB meteorites, 2 winonaites and K-Ar ages of Toluca and Four Corners range from 4.32 to 4.55 Ga (Podosek 1970; Niemeyer 1979a, 1979b; Benedix et al. 1998; Takeda et al. 2000; Bogard et al. 1968, 2005). In all IAB meteorites studied so far, I-Xe ages are generally older, from 4.5579 ± 0.0001 to 4.5762 ± 0.0024 Ga (Podosek 1970; Niemeyer 1979a; Bogard et al. 2005). The I-Xe ages reported by Niemeyer (1979a) are among the oldest, seeming to predate the Pb-Pb ages of CAIs by about 7 Ma (Chen et al. 1981; Göpel et al. 1991; Amelin et al. 2002). It has been established that proper irradiation monitors are essential in I-Xe dating (Hohenberg et al. 2000; Pravdivtseva et al. 2003; Hohenberg and Pravdivtseva 2008). Niemeyer (1979a) analyzed three independent flux monitors: KI salt, and two meteorites St. Séverin and Bjurböle. Both St. Séverin and Bjurböle yielded disturbed correlation lines, and three aliquots of KI gave "badly discrepant results" (Niemeyer 1979a). Moreover, it was shown later that St. Séverin has two distinct lithologies with I-Xe age difference of 6.8 Ma (Hohenberg et al. 1981). Pure iodine compounds are not appropriate as I-Xe monitors, as discussed by Hohenberg and Pravdivtseva (2008), since the sharp resonances in the neutron capture cross sections of ^{127}I lead to self-shielding. This uncertainty in the absolute age, caused by the deficiencies of the monitors, could be responsible for the old ages reported by Niemeyer (1979a). Even without this set of seven ages, the remaining five I-Xe absolute ages are consistently older then corresponding Ar-Ar ages.

Bogard et al. (2005) suggested two possible explanations for this age discrepancy in IABs and winonaites: That the I-Xe system in IAB meteorites was not reset during early parent body breakup and reassembly, or that there is a bias in the decay parameters for ^{40}K, with the renormalized Ar-Ar ages for most meteorites about 30 Ma older (Renne 2000; Trieloff

et al. 2003). While a revised decay constant can address an age bias between I-Xe and Ar-Ar, it cannot address the observed age spread. When the revised ^{40}K decay constant (Mundil et al. 2006) is applied in recent work by Vogel and Renne (2008), the resulting Ar-Ar ages of silicates from the IAB irons Caddo County, Campo del Cielo, Landes and Ocotillo are closer to that of I-Xe in some cases, they still demonstrate a wide range of absolute ages from 4562 ± 20 Ma (Caddo County) to 4362 ± 40 Ma (Campo del Cielo). These ages did not correlate with grain sizes or "quality" grades of the plagioclase separates studied. It led the authors to the conclusion that IAB silicate Ar-Ar ages should depend much more on the pre- and post-impact cooling rates and on burial depth than on the time of the actual impact. However, the more retentive I-Xe ages, which tend to cluster at ~4560 Ma for these objects, could more closely reflect the closure time after catastrophic impact and reassembly of the IAB parent body.

Toluca Cooling Rate

I-Xe ages from this work provide different closure times for the high and low-Mg pyroxenes in Toluca. Although the isochrons in these grains are based on all released Xe (correlated and uncorrelated), the effect of uncorrelated Xe has been evaluated and minimized. Even with the uncertainty of uncorrelated Xe, the age differences derived for these two groups of Toluca pyroxenes are clearly defined. This age difference and the mineralogical properties of these two grain types form the basis for determination of the cooling rate.

Although the actual closure temperatures for Xe in high- and low-Mg pyroxenes are not known with certainty, it is the difference in closure temperatures that provides the cooling rate. For a zeroth order estimate of cooling rate, the differences in melting temperatures of these two minerals might be used. The melting temperature for enstatite, $MgSiO_3$, is 1557 °C (Lodders and Fegley 1998). Crystallization of protoenstatite from a melt was observed at 1564 ± 2 °C, with the subsequent transformation of this unquenchable phase into clinoenstatite after rapid cooling (Nikitin 1948). Crystallization temperatures for low-Mg pyroxenes could be deduced from the parameters of the controlled-gas quench furnace synthesis of Ca-Mg-Fe pyroxenes (Turnock et al. 1973). It was observed that pyroxenes with Mg number less than 0.50 will melt if synthesized at 1200 °C (atmospheric pressure), standard heating temperature for the synthesis of pyroxenes with higher Mg numbers. Thus all low-Mg synthesis experiments were conducted at 1150 °C to avoid melting.

The relationship between the crystallization temperature and the Mg and Fe concentrations in the enstatite-ferrosilite solid solution series is difficult to establish and the linear approximation used here is for the 1.0–0.5 Mg number range, not for the whole enstatite-ferrosilite solid solution series. Using the crystallization temperatures for known components (Lodders and Fegley 1998; Turnock et al. 1973), a linear relationship *Temperature = 728 × (Mg-number) + 836* can be established for intermediate compositions with Mg-numbers in the 1.00–0.50 range. The temperatures provided by this relationship are 1345 to 1441 °C for low-Mg pyroxenes and 1486 to 1545 °C for high-Mg pyroxenes. Using the two group averages, 1393 ± 48 °C and 1516 ± 29 °C, respectively, the difference in closure temperature is 123 ± 56 °C. With the 123 ± 56 °C temperature interval and the corresponding 8.5 ± 4.4 Ma age difference, the cooling rate at the time of silicate exsolution in Toluca (presumably after breakup and reassembly of parent body) is found to be 14.5 ± 10.0 °C/Ma. Although the linear approximation may allow us to estimate the difference in closure temperature for the I-Xe system in high- and low-Mg silicates with better precision, it is still the major contributor to the cooling rate uncertainty.

It was first shown by Tammann (1926) that the diffusion properties of iron oxides and silicates change in a narrow range of temperatures, a factor of 0.5–0.52 below their melting temperatures. This, the so called Tammann temperature, represents the commencement of significant self-diffusion. In this case the Tammann temperature corresponds to 724 ± 17 °C and 788 ± 48 °C for the low- and high-Mg pyroxenes, respectively, leading to an apparent cooling rate of about 7.5 °C/Ma. While such solid-state mobility may be the operative mechanism for the onset of diffusion of small chemically-active atoms, it may not accurately reflect the initiation of diffusion for the large inert Xe atoms within a crystal lattice. In fact, it has been independently shown that the I-Xe chronometer is less susceptible to resetting by thermal events than chronometers based upon chemically active species, such as Pb-Pb (Pravdivtseva et al. 2004) so the Tammann temperature may not be as applicable as the crystallization temperature for Xe closure in these minerals. The uncertainty of cooling rate derived from the difference in crystallization temperatures (14.5 ± 10.0 °C/Ma) overlaps the cooling rate derived from the difference in Tammann temperatures.

A metallographic cooling rate for Toluca was first estimated by Wood (1964) and later determined to be 25 ± 15 °C/Ma (Saikumar and Goldstein 1988). In the Saikumar and Goldstein model, the interface between the kamacite and taenite was only allowed to move in one direction, to deplete the taenite phase, and diffusion in the kamacite phase was assumed to be infinitely fast at temperatures above ~450 °C. In a later model by Hopfe and Goldstein (2001), the movement of the kamacite/taenite interface was allowed in either direction, and kamacite growth in the temperature interval 700–200 °C for Toluca was simulated for several linear cooling rates and number of impingement lengths to develop appropriate curves using the Wood method. Although the Wood curves from the Hopfe and Goldstein model seem to provide a better fit to the experimental data,

that model still yields the same cooling rate for Toluca, 25 °C/Ma, as reported earlier (Saikumar and Goldstein 1998), but now with a more realistic feel for the uncertainty, now listed as a factor of 2 (Hopfe and Goldstein 2001).

CONCLUSION

According to the ^{207}Pb-^{206}Pb data, calcium-aluminum inclusions from Efremovka (CV3) and Allende (CV3) are the oldest of solar system solids, formed at 4567.2 ± 0.6 Ma (Chen et al. 1981; Göpel et al. 1991; Amelin et al. 2002). The ^{207}Pb-^{206}Pb ages of chondrules range from 4566.7 ± 1.0 Ma for Allende (CV3) to 4564.7 ± 0.7 Ma for Acfer 059 (CR2), 4562.7 ± 1.7 Ma for Richardton (H5) and 4562.7 ± 0.5 Ma for Gujba (CBa) (Amelin et al. 2004; Amelin et al. 2005). Although the I-Xe ages for chondrules from different types of ordinary chondrites have a real spread, reflecting their complicated metamorphic histories, the oldest chondrules from the most primitive of these, Bjurböle, Richardton and Semarkona, cluster tightly at about 1.8 ± 1.8 Ma after formation of CAIs (Hohenberg and Pravdivtseva 2008). These observations suggest that if indeed the Pb-Pb age of the Gujba chondrule reflects its formation time, as was argued by Amelin et al. (2004), the protoplanetary nebula still existed 4.5 Ma after formation of the oldest known solids. Based on the constraints available from long- and short-lived chronometers, Wadhwa et al. (2006) concluded that differentiation of planetesimals in the early history of the solar system occurred quite rapidly. Melting on some planetesimals was initiated as early as ~3–5 Ma after formation of the first solids and extended to more than ~10 Ma on others. According to the model proposed by Benedix et al. (2000), partial melting and metamorphism are crucial for the formation of IAB meteorites and appears to have produced five different lithologies. In that model, after breakup the reassembly resulted in a range of compositions forming the complex set of IAB meteorites. Benedix et al. (2000) suggested that some metallic melt bodies either remained intact or were not thoroughly mixed with silicate material during parent-body breakup and reassembly. This suggestion is supported by the occurrence of rounded, graphite-troilite-rich, silicate-poor inclusions found in Toluca, that almost certainly formed by exsolution from the still molten metal (Buchwald 1975). Silicates studied in this work were separated from one of such inclusion. If indeed this Toluca graphite-troilite-rich inclusion formed after the breakup and reassembly of the IAB parent body, the I-Xe age of the high-Mg pyroxenes separated from this inclusions indicate that this catastrophic impact occurred not later than 4560.5 ± 2.4 Ma, 6.7 Ma after formation of CAIs, in good agreement with time-scale estimates of planetesimals formation and differentiation (Wadhwa et al. 2006).

The cooling rate at the time of silicate exsolution in Toluca after breakup and reassembly of the IAB parent body is measured here to be 14.5 ± 10.0 °C/Ma, in agreement with the metallographic cooling rates found by Herpfer et al. (1994) and Hopfe and Goldstein (2001). More precise results can be expected when the mineral compositions and thus crystallization temperatures are more rigidly constrained but even these results provide further reassurance that closure temperature differences can be accurately estimated even if the actual closure temperatures are more elusive.

Acknowledgments–The authors thank Dr. Katharina Lodders for helpful suggestions, Prof. Joseph I. Goldstein for encouragement, productive discussion and comments during preparation of this manuscript; and Dr. Tim Swindle, Dr. Gretchen Benedix, and Dr. Alexis Busfield for providing helpful reviews. This work supported, in part, by NASA grant #NNG06GE84G.

Editorial Handling—Dr. Timothy Swindle

REFERENCES

Amelin Y., Krot A. N., Hutcheon I. D., and Ulyanov A. A. 2002. Lead isotopic ages of chondrules and calcium-aluminum-rich inclusions. *Science* 297:1678–1683.

Amelin Y., Krot A., and Twelker E. 2004. Pb isotopic age of the CB chondrite Gujba, and the duration of the chondrule formation interval. *Geochimica et Cosmochimica Acta* 68:11, Supplement 1, A759.

Amelin Y., Ghosh A., and Rotenberg E. 2005. Unraveling the evolution of chondrite parent asteroids by precise U-Pb dating and thermal modeling. *Geochimica et Cosmochimica Acta* 69: 505–518.

Benedix G. K., McCoy T. J., Keil K., Bogard D. D., and Garrison D. H. 1998. A petrologic and isotopic study of winonaites: Evidence for early parent body partial melting, brecciation, and metamorphism. *Geochimica et Cosmochimica Acta* 62:2535–2553.

Benedix G. K., McCoy T. J., Keil K., and Love S. G. 2000. A petrologic study of the IAB iron meteorites: Constraints on the formation of the IAB-Winonaite parent body. *Meteoritics & Planetary Science* 35:1127–1141.

Bogard D. D., Burnett D. S., Eberhardt P., and Wasserburg G. J. 1968. ^{40}Ar-^{40}K ages of silicate inclusions in iron meteorites. *Earth and Planetary Science Letters* 3:275–283.

Bogard D. D., Garrison D. H., and Takeda H. 2005. Ar-Ar and I-Xe ages and the thermal history of IAB meteorites. *Meteoritics & Planetary Science* 40:207–224.

Buchwald V. F. 1975. *Handbook of iron meteorites.* University of California Press. 1418 p.

Chen J. H., and Wasserburg G. J., 1981. The isotopic composition of uranium and lead in Allende inclusions and meteoritic phosphates. *Earth and Planetary Science Letters* 52:1–15.

Drebushchak V. A., Kovalevskaya Yu. A., Paukov I. E., and Surkov N. V. 2008. Low-temperature heat capacity of monoclinic enstatite. *Journal of Thermal Analysis and Calorimetry* 94:493–497.

Gilmour J. D., Pravdivtseva O. V., Busfield A., and Hohenberg C. M. 2004. I-Xe and the chronology of the early solar system. Workshop on Chondrites and the Protoplanetary Disk, Abstract #9054.

Gilmour J. D., Pravdivtseva O. V., Busfield A., and Hohenberg C. M. 2006. The I-Xe chronometer and the early solar system. *Meteoritics & Planetary Science* 41:19–41.

Göpel C., Manhes G., and Allegre C. J. 1991. Constraints on the time of accretion and thermal evolution of chondrite parent bodies by precise U-Pb dating of phosphates. *Meteoritics & Planetary Science* 26:A338.

Herpfer M. A. 1988. The silicate inclusions of group IAB iron meteorites: Implications for metal-silicate segregation and core formation. M.S. thesis, Arizona State University, USA.

Herpfer M. A., Larimer J. W., and Goldstein J. I. 1994. A comparison of metallographic cooling rate methods used in meteorites. *Geochimica et Cosmochimica Acta* 58:1353–1365.

Hohenberg C. M. 1980. High sensitivity pulse-counting mass-spectrometer system for noble gas analysis. *Review of Scientific Instrum*ents 51:1075–1082.

Hohenberg C. M. and Pravdivtseva O. V. 2008. I–Xe dating: From adolescence to maturity. *Chemie der Erde* 68:339–351.

Hohenberg C. M., Hudson B., Kennedy B. M., and Podosek F. A. 1981. Noble gas retention chronologies for the St. Séverin meteorite. *Geochimica et Cosmochimica Acta* 45:535–546.

Hohenberg C. M., Pravdivtseva O. V., and Meshik A. P. 2000. Reexamination of anomalous I-Xe ages: Orgueil and Murchison magnetites and Allegan feldspar. *Geochimica et Cosmochimica Acta* 64:4257–4262.

Hohenberg C. M., Pravdivtseva O. V., and Meshik A. P. 2004. Trapped Xe and I-Xe ages in aqueously altered CV3 meteorites. *Geochimica et Cosmochimica Acta* 68:4745–4763.

Hopfe W. D. and Goldstein J. I. 2001. The metallographic cooling rate method revised: Application to iron meteorites and mesosiderites. *Meteoritics & Planetary Science* 36:135–154.

Lavielle B. and Marti K. 1992. Trapped xenon in ordinary chondrites. *Journal of Geochemical Research* 97:875–881.

Lodders K., Fegley B. Jr. 1998. *The planetary scientist's companion*. New York: Oxford University Press. 380 p.

McDougall I. and Harrison T. M. 1999. *Geochronology and thermochronology by the $^{40}Ar/^{39}Ar$ method*, 2nd ed. New York: Oxford University Press. 269 p.

Mundil R., Renne P. R., Min K., and Ludwig K. R. 2006. Resolvable miscalibration of the $^{40}Ar/^{39}Ar$ geochronometer. *Eos Transactions*, Fall Meet. Suppl., Abstract V21A–0543.

Niemeyer S. 1979a. I–Xe dating of silicate and troilite from IAB iron meteorites. *Geochimica et Cosmochimica Acta* 43:843–860.

Niemeyer S. 1979b. ^{40}Ar–^{39}Ar dating of inclusions from IAB iron meteorites. *Geochimica et Cosmochimica Acta* 43:1829–1840.

Nikitin V. D. 1948. Equilibrium diagram of the systems magnesia-silica. From *Izvestiya Sektora Fiziko-Khimicheskogo Analiza, Institut Obshchei i Neorganicheskoi Khimii, Akademiya Nauk SSSR* 16:29–46.

Podosek F. A. 1970. Dating of meteorites by the high temperature release of iodine-correlated ^{129}Xe. *Geochimica et Cosmochimica Acta* 34:341–366.

Pravdivtseva O. V., Hohenberg C. M., and Meshik A. P. 1998. Distribution of radiogenic ^{129}Xe among individual mineral grains of iron meteorites. 29th Lunar and Planetary Science Conference. Abstract #1818.

Pravdivtseva O. V., Hohenberg C. M., and Meshik A. P. 2003. The I-Xe age of Orgueil magnetite: new results. 34th Lunar and Planetary Science Conference. Abstract #1863.

Pravdivtseva O. V., Amelin Yu., Meshik A. P., and Hohenberg C. M. 2004. I-Xe and Pb-Pb ages of individual Elenovka (L5) chondrules. Proceedings, 14th Annual Goldschmidt Conference. *Geochimica et Cosmochimica Acta* 68:A760.

Renne P. R. 2000. $^{40}Ar/^{39}Ar$ age of plagioclase from the Acapulco meteorite and the problem of systematic errors in cosmochronology. *Earth and Planetary Science Letters* 175: 13–26.

Saikumar V. and Goldstein J. I. 1988. An evaluation of the methods to determine the cooling rates of iron meteorites. *Geochimica et Cosmochimica Acta* 52:715–726.

Schultz L. and Franke L. 2000. Helium and argon in meteorites: A data collection unpublished compilation: At www.mpck-mainz.mpg.de/~kosmo/schultz.htm.

Scott E. R. D. 2004. Meteoritic constrains on collisional rates in the primordial asteroid belt and its origin. 35th Lunar and Planetary Science Conference. Abstract #1990.

Takeda H., Bogard D. D., Mittlefehldt D. W., and Garrison D. H. 2000. Mineralogy, petrology, chemistry and ^{39}Ar–^{40}Ar and exposure ages of the Caddo County IAB iron: Evidence for early partial melt segregation of gabbro area rich in plagioclase-diopside. *Geochimica et Cosmochimica Acta* 64:1311–1327.

Tammann G. 1926. The temperature of the beginning of inner diffusion in crystals. *Zeitschrift für Anorganische und Allgemeine Chemie* 157:321.

Trieloff M., Jessberger E. K., Herrwerth I., Hopp J., Fiéni C., Ghélis M., Bourot-Denise M., and Pellas P. 2003. Structure and thermal history of the H chondrite parent asteroid revealed by thermochronometry. *Nature* 422:502–506.

Turnock A. C. Lindsley D. H., and Grover J. E. 1973. Synthesis and unit cell parameters of Ca-Mg-Fe pyroxenes. *American Mineralogist* 58:50–59.

Vogel N. and Renne P. 2008. ^{40}Ar–^{39}Ar dating of plagioclase grain size separates from silicate inclusions in IAB iron meteorites and implications for the thermochronological evolution of the IAB parent body. *Geochimica et Cosmochimica Acta* 72:1231–1255.

Wadhwa M., Srinivasan G., and Carlson R. W. 2006. Time scales of planetesimal differentiation in the early solar system. In *Meteorites and the early solar system II,* edited by Lauretta D. S. and McSween H. Y. Jr. Tucson: The University of Arizona Press. pp. 715–732.

Wasson J. T. and Kallemeyn G. W. 2002. The IAB iron-meteorite complex: A group, five subgroups, numerous grouplets, closely related, mainly formed by crystal segregation in rapidly cooling melts. *Geochimica et Cosmochimica Acta* 66:2445–2473.